

# Preparation of N-, S-Co-Doped Activated Carbons Derived from Waste Medium Density Fiberboard for Supercapacitors

Ruquan Ren, Tongxin Shang, Xiaojuan Jin \* and Jianmin Gao\*

Nitrogen-, sulfur-co-doped activated carbons were obtained from sulfur-modified and nitrogen-doped activated carbons that were prepared from waste medium density fiberboard. The electrochemical capacitive performance of the activated carbon samples obtained was investigated in 7.0 M KOH electrolyte. The morphology, structure, and surface properties of the samples were investigated by field emission scanning electron microscopy (FESEM), transmission electron microscopy (TEM), N<sub>2</sub> adsorption, X-ray photoelectron spectroscopy (XPS), and elemental analysis. The S-doping could be tuned by controlling the dosage of sulfur sublimed. Because of the introduction of sulfur functional groups, the prepared carbons exhibited better conductivity and higher specific capacitance, reaching 264 F/g under a current density of 50 mA/g and a 7.0 mol/L KOH electrolytic solution. A mechanism for improving the conductivity and capacitive performance of sulfur functional groups on activated carbons was discussed.

*Keywords:* N, S-co-doped activated carbons; Waste medium density fiberboard; Sulfur functional groups

*Contact information:* Beijing Key Laboratory of Lignocellulosic Chemistry, MOE Engineering Research Center of Forestry Biomass Materials and Bioenergy, Beijing Forestry University, 35 Qinghua East Road, Haidian, 100083, Beijing, China; \*Corresponding author: jxj0322@163.com (Xiaojuan Jin); gaojm@bjfu.edu.cn (Jianmin Gao)

## INTRODUCTION

Electrochemical supercapacitors, which can be divided into electrochemical double layer capacitors (EDLCs) and pseudo-capacitors, have incurred universal research interest as energy storage devices because of their high power density, long lifecycle, and reversibility. Electrochemical double layer capacitors are based on the accumulation of charges at the electrode/electrolyte interface; therefore, capacitance is strongly dependent on the surface area of the electrode material. Pseudo-capacitors make use of a reversible redox reaction to store charge, and the charge storage mechanism is faradic because the charge passing across the double layer is integral to the workings of the devices (Djurfors *et al.* 2003; Huang *et al.* 2014). Electrical conductive polymers and metal oxides, common pseudo-capacitive materials, have shown high specific capacitance. However, high price, low conductivity, and poor cycle capacity have limited their practical application as pseudo-capacitive materials (Si *et al.* 2013).

Activated carbons (ACs) are starting materials for EDLCs because of their electrochemical inertness, high electrical conductivity, large specific surface area, and good adsorption property. The electrochemical performance of EDLCs is dependent upon the surface area, pore structure, and surface chemistry of the activated carbons. Therefore, ACs, with a high specific surface area, are expected to be applied as electrode

materials to enhance EDLCs with high performance (Faraji and Ani 2015). However, the EDLCs cannot be enhanced illimitably because the excessive increase in surface area would result in the decrease of mesoporosity, resulting in a reduction in the mass transfer capacity. It is desirable to improve the EDLCs capacitance by introducing Faradaic redox reaction without sacrificing of cycling stability (Sari and Ting 2015). The introduction of heteroatoms to ACs, such as nitrogen (N), phosphorus (P), sulfur (S), and boron (B), is suitable for combining the advantages of pseudo-capacitance with high surface area carbon (Tsubota *et al.* 2011). Activated carbons, modified with nitrogen heteroatoms, have attracted much interest because nitrogen functional groups were found to improve the wettability of the carbon network and contribute to pseudo-capacitance through faradic reactions. Zhou *et al.* (2014) reported that N-doped porous carbon capsules with tunable porosity were high-performance supercapacitors, and Shang *et al.* (2015) also studied the mechanism of nitrogen functional groups of carbon materials.

Sulfur has a lone pair of electrons, which could introduce pseudo-capacitance to carbon by the incorporation of S functional groups in the carbon framework. It has also been reported that S-doped activated carbons exhibit higher specific capacitance than plain activated carbons. Hasegawa *et al.* (2011) first reported that S-doped carbon could be used as a supercapacitor electrode material because of the redox faradic reactions provided by the additional sulfur-containing functional groups. Consequently, the specific capacitance of the carbon material was increased by 38% in an aqueous system compared with the conventional-ordered mesoporous carbon in their research. Huang *et al.* (2014) produced sulfurized activated carbons by coating the pore surface with thiophenic sulfur functional groups from the pyrolysis of sulfur flakes. Sulfurized activated carbon electrodes exhibit better conductivity and increased specific capacitance that is almost 40% higher than plain activated carbon electrodes at a high current density of 1.4 A/g. The addition of thiophene and sulfone species enhance faradic reactions and improve the specific capacitance of carbon in aqueous electrolytes, according to previous research (Sevilla and Fuertes 2012; Gu *et al.* 2013; Huang *et al.* 2014; Zhou *et al.* 2014). Zhao *et al.* (2012) also explored the idea of sulfoxide-, aromatic sulfide-, and sulfone-mediated mesoporous carbon for supercapacitors (Zhao *et al.* 2012).

Activated carbons produced from natural materials such as different biomasses are an attractive and economic option for use as electrode materials (Inal *et al.* 2015). Waste medium density fiberboard (MDF), as reported by Shang *et al.* (2014), is a good material for supercapacitors. Medium density fiberboard contains many nitrogen atoms, which originate from urea-formaldehyde resin. The recycling of MDF represents an efficient and environmentally friendly way to utilize this waste material.

In this work, N-, S-co-doped activated carbon was made by coating the pore surface of nitrogen-doped activated carbon with sulfur functional groups from the pyrolysis of sublimed sulfur. In this manner, nitrogen and sulfur species could be introduced into the target carbon materials. The performance of N-, S-co-doped activated carbon was investigated as an electrochemical capacitor. Additionally, the effects of sulfur on MDF electrochemical performance are discussed in detail.

## EXPERIMENTAL

### Materials

The waste MDF was provided by the Jiahekailai Furniture and Design Company, in Beijing, China. Other chemicals were purchased from the Beijing Yixiubogu Chemical Reagent Co. (Beijing, China). All chemicals were of analytical grade, and the solutions were prepared with distilled water.

### Preparation of Activated Carbon

The carbonization process was conducted according to Shang *et al.* (2014). In the activation step, 3.0 g of the oven-dried samples was mixed with KOH at a mass ratio impregnation of (3:1). The samples were then activated at the temperature of 800 °C for 1 h in a nitrogen atmosphere. Then, the activated carbons were boiled with 1.0 M HCl solution and then with distilled water until the pH of the solution reached approximately 6 to 7. Thereafter, samples were dried at 115 °C in an oven for 4 h. The obtained activated carbon samples and sublimed with sulfur at a weight ratio of 6:1, 8:1, 10:1, and 12:1. Then, the samples were mixed with agate mortar and pestle ground into uniform powders. Then, the mixture was heat-treated at 400 °C for 2 h, with a heating rate of 5 °C/min under a nitrogen atmosphere with a flow rate of 10 mL/min. The heat-treated samples were referred to as AC6, AC8, AC10, and AC12, depending on the ratio of activated carbon to sublimed sulfur, which were 6:1, 8:1, 10:1, and 12:1, respectively. The sample that was not sulfur-modified was referred to as AC. Finally, the activated carbons (AC, AC6, AC8, AC10, and AC12) were dried at 115 °C in an oven for 4 h.

### Characterization of the Activated Carbons

Through elemental analysis, the content of carbon (C), hydrogen (H), N, and S were determined using a CHN analyzer (Thermo Finnigan Flash, EA 1112 series, Thermo Fisher Scientific, Waltham, MA). X-ray photoelectron spectroscopy (XPS) was used to determine the surface functional groups of the samples. The acceleration tension and power of the X-ray source were 15 kV and 100 W, respectively.

Surface morphologies from cross sections of the samples were observed using field emission scanning electron microscopy (FESEM; JSM-7000, JEOL Ltd., Tokyo, Japan). Transmission electron microscopy (TEM) measurements were conducted on a JEM-1010 transmission electron microscope (JEOL Ltd, Japan).

The pore volume, pore diameter, and Brunauer Emmett-Teller (BET) surface area of the samples were determined from the corresponding N<sub>2</sub> adsorption-desorption isotherms obtained at -196 °C with an accelerated surface area and porosimetry system (ASAP 2010, Micromeritics Instrument Corp., Atlanta, GA). The BET method was used to determine the specific surface area ( $S_{BET}$ ). The total pore volume was calculated from the N<sub>2</sub> adsorption isotherm at a relative pressure of 0.995 (P/P<sub>0</sub>). For the micropore volume and mesoporous surface area, the V-t and Barrett-Joyner-Halenda (BJH) methods were used, respectively. The pore size distribution was calculated using the density functional theory (DFT).

### Electrode Preparation and Electrochemical Measurements

Electrodes for electrochemical measurements were prepared from the samples by first grinding the particles into fine powders. The measurements were fabricated by mixing the samples with acetylene black and 60% polytetrafluoroethylene at the mass

ratio of 87:10:3. Then, the mixture was coated onto a nickel foam substrate square (1.0 cm<sup>2</sup>) and dried in an oven at 115 °C for over 4 h. All electrochemical tests were carried out using two-electrode cells in 7.0 mol/L KOH electrolyte on the BT 2000 battery testing system (Arbin Instruments, College Station, TX, USA) and the 1260 electrochemical workstation (Solartron Metrology, West Sussex, UK).

## RESULTS AND DISCUSSION

### Elemental Analysis and XPS Study

Table 1 shows the elemental analysis of the samples. After modification, there was an increase in the presence of sulfur contents with increasing sulfur dosage. The sulfur content of N-, S-co-doped activated carbons (SAC) ranged from 1.45% to 1.93%, indicating the presence of sulfur in the SAC samples after the heat-treatment, and a partial loss of sulfur, which could have been attributed to evaporative losses during the heating process. The nitrogen content of the samples was similar, ranging from 1.13% to 1.19%. This suggested that a portion of the nitrogen atoms were turned over (some of the nitrogen atoms of the waste MDF originate from urea-formaldehyde resin adhesive used in the MDF manufacturing process, and they are further turned over to waste MDF-based ACs) to the obtained samples, and that the nitrogen-containing functional groups weren't damaged during the modification process.

To obtain further information about the surface chemistry of the samples, the surface elemental composition of the samples was investigated by XPS (Table 2, Fig. 1). Many researchers have reported the action mechanism of nitrogen-containing functional groups for improving electrochemical performance (Nolan *et al.* 2013; Shang *et al.* 2014; Ferrero *et al.* 2015; Shang *et al.* 2015; Wang *et al.* 2016; Gao *et al.* 2016). The nitrogen species of the carbon matrix include pyridinic (N-6), pyrrolic/pyridone (N-5), quaternary nitrogen (N-Q), and pyridine-N-oxide (N-X). The relative contributions of each nitrogen species to the total peak area are summarized in Table 2. According to a previous work by the authors (Shang *et al.* 2014), there are three nitrogen species (N-6, N-5, N-X) in the activated carbon derived from waste medium density fiberboard. Thus, the chemical state of nitrogen could be sensitively varied by the carbonization temperature and activation temperature. According to the analysis the optimum experimental conditions are 500 °C for carbonization temperature and 800 °C for activation temperature. After modification, the photoemission spectrum of AC10 did not show the obvious intensity change of C1s and O1s compared with the AC sample, because the tunable SAC samples were obtained by controlling the dosage of sublimed sulfur. Table 2 reveals the existence of three types of sulfur functionalities at the binding energies of S<sup>2-</sup> (sulfide) (161.4 to 161.6 eV), thiophene (163.9 to 164.5 eV), and sulfone (168.0 to 168.9 eV). Eventually, a small amount of sulfur in the AC sample formed the main sulfur species: -C-S-C- thiophene and -C-S(O)<sub>2</sub>-C- sulfone bridges (Fig. 2). According to the XPS analysis, sulfur atoms in the SAC samples were incorporated into the carbon framework through the formation of C-S and C-SO<sub>2</sub>-C bonds to produce similar thiophene and sulfone bridge structures. The increased capacitance of the SAC samples was primarily attributed to the thiophene functional groups (Huang *et al.* 2014; Zhou *et al.* 2014). This type of structure is characterized by a lone electron pair among the sulfur atom *p*-orbital overlapping with  $\pi$ -orbitals of the graphite sp<sup>2</sup> hybridization, forming an extended  $\pi$ -system with a filled valence band that is conjugated with the backbone carbon structure. Surface electron density of SAC samples was higher because of the synergistic activation of conjugated

carbon in combination with the electron-rich sulfur groups, thus increasing of dipole moment. According to the “like-dissolves-like” theory, the total polarization of the medium would enlarge as a result of the enhanced dipole moment, which could facilitate the penetration of polar substrate into the pores (Zhao *et al.* 2012). Additionally, sulfone bridges, resulting from the oxidative conditions, could also participate in faradic reactions and improve the specific capacitance of carbon.

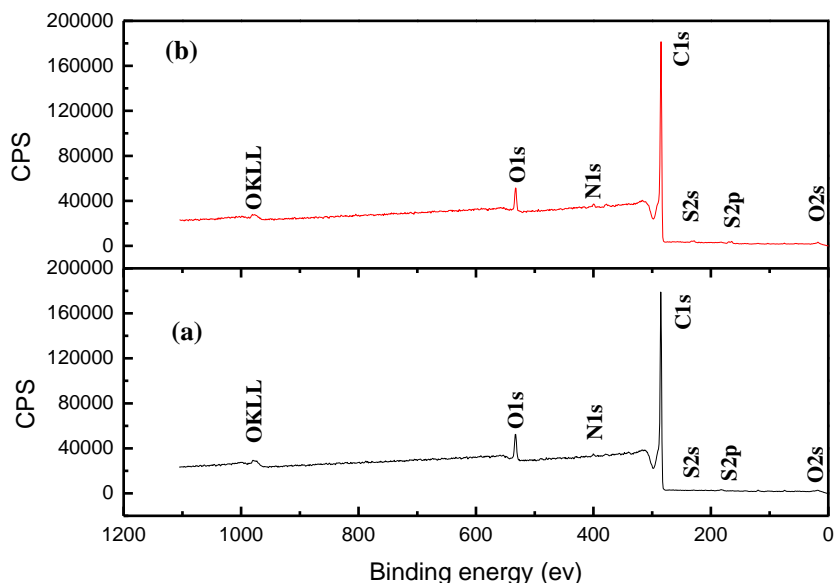


Fig. 1. XPS curves (XPS full spectrum scanning) (a) AC and (b) AC10

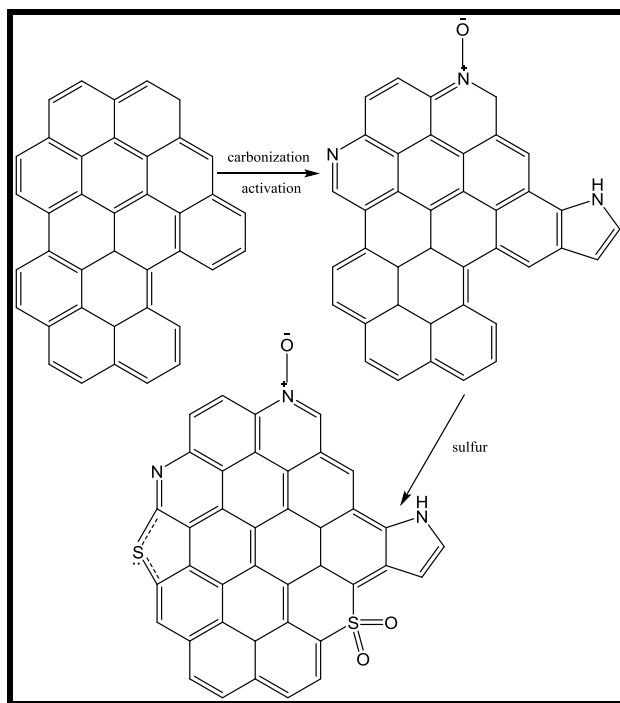


Fig. 2. Chemical structure of sulfur-containing functional groups

**Table 1.** Elemental Analysis of the Samples

Sample	C, H, N, S (wt.%)			
	C (%)	H (%)	N (%)	S (%)
AC	91.04	0.19	1.19	0.03
AC12	91.91	0.17	1.17	1.45
AC10	91.39	0.12	1.14	1.64
AC8	91.77	0.16	1.13	1.79
AC6	91.27	0.15	1.16	1.93

**Table 2.** Detailed XPS Analysis of the Samples

Sample	AC12	AC10	AC8	AC6	AC
N surface concentration (%)					
N-6, pyridinic nitrogen (%)	24.2	26.1	27.9	25.7	25.5
N-5/N-P, pyrrolic nitrogen, pyridine (%)	59.3	58.5	56.2	57.1	58.3
N-X, oxidized nitrogen (%)	16.5	15.4	15.9	17.2	16.2
S surface concentration (%)					
S <sup>2-</sup> (sulfide) (%; 161.4 to 161.6 eV)	7.8	8.1	6.7	7.9	47.6
Thiophene (%; 163.9 to 164.5 eV)	49.2	47.7	50.8	45.8	14.3
Sulfone (%; 168.0 to 168.9 eV)	43.0	44.2	42.5	46.3	38.1

### Textural Studies of Samples

Figure 3 shows FESEM and TEM images of AC and AC10 samples. The surface morphologies of AC and AC10 were similar, and the AC10 sample retained its porous structure, even after the modification with sulfur. Honeycomb structures resulting from the chemical activation process are visible in the FESEM images. Continuous pores structure can be seen from TEM images; the darker regions represent the carbon frame and the pores are shown as white areas. The results of FESEM and TEM analysis reveal that both mesopores and micropores were present in the activated carbon.

Porous structures in the samples were determined by BET analysis (Fig. 4). The surface area and pore volume, calculated according to the DFT ( $V_{dir}$ ) method, are listed in Table 3. According to the International Union of Pure and Applied Chemistry (IUPAC) classification, all isotherms presented a combination of type-I and type-II isotherms, which indicate that all of the samples possessed a combination of microporous and mesoporous structure. In addition, Fig. 4 shows a slight hysteresis loop (type IV) in the desorption branch, at a relative pressures of approximately 0.9 units ( $P/P_0$ ). This may indicate the presence of mesopores. A similar character could be concluded from the pore size distribution curves in Fig. 5. Apparently, the AC sample had a total surface area of 2081 m<sup>2</sup>/g, and after coating with sulfur, the total surface area showed an obvious decrease for all four SAC samples. Meanwhile, both the mesopore and micropore surface

areas were decreased by differing amounts. These reductions could have resulted from the effect that the sulfur coating had on the surface of the pores. The sulfur coating could have penetrated the mesopores and micropores, causing blockages in the pore structure, which resulted in the notable decrease in the  $S_{BET}$  and adsorption property.

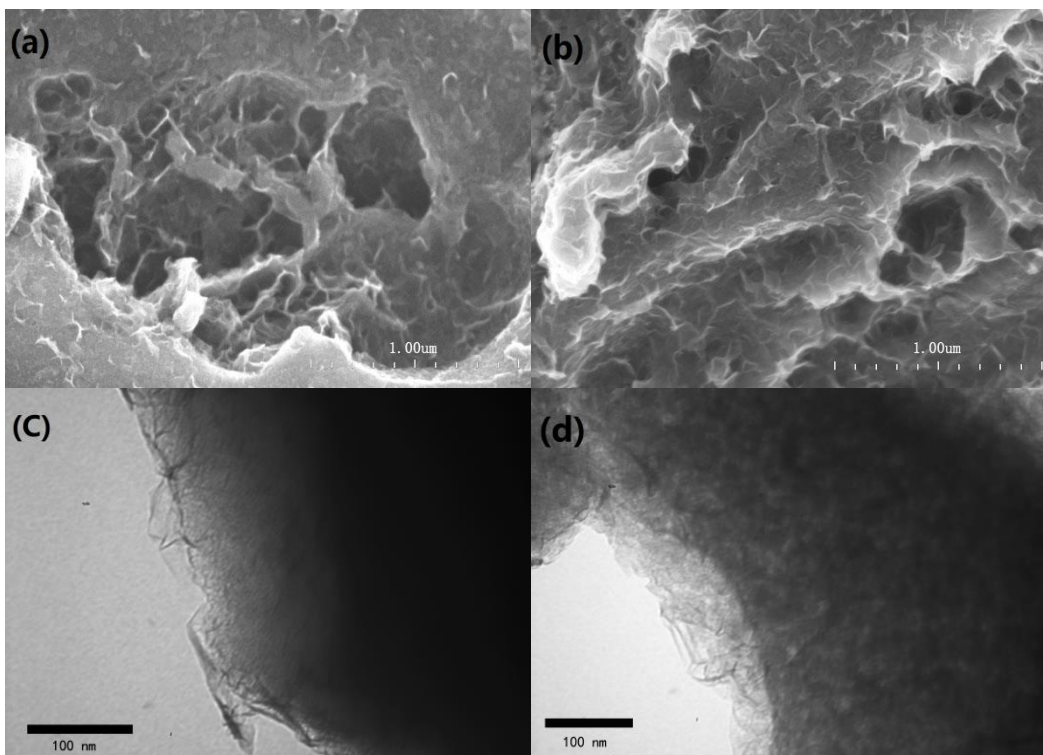


Fig. 3. FESEM of the (a) AC and (b) AC10; TEM images of (c) AC and (d) SAC

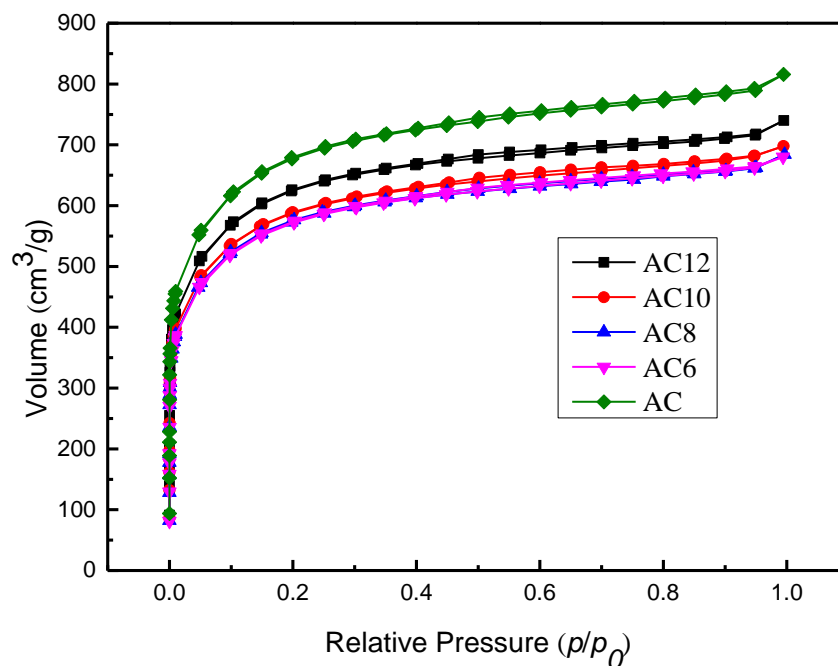
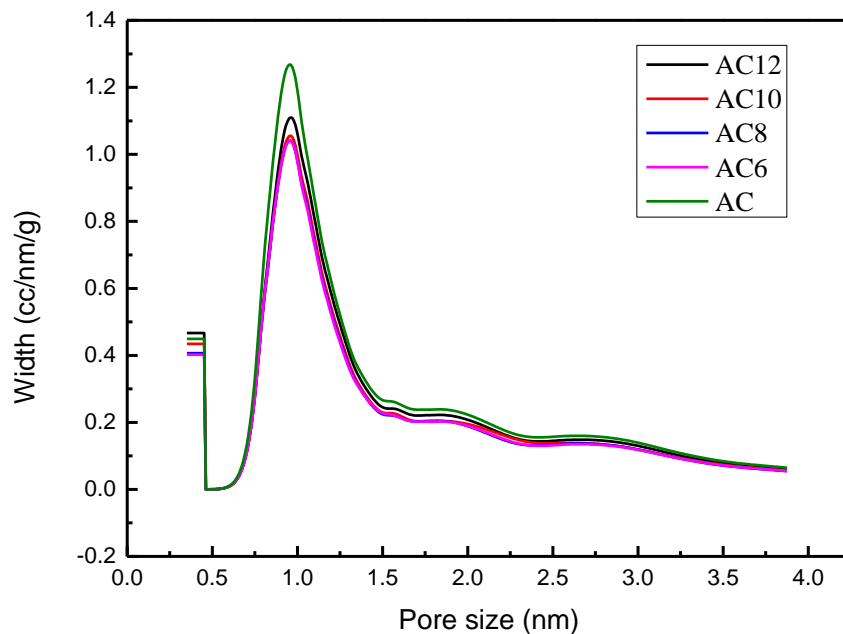


Fig. 4. Nitrogen adsorption–desorption isotherms of the samples



**Fig. 5.** Pore size distribution of the prepared activated carbons

**Table 3.** Physical Properties of the Samples

Sample	$S_{\text{BET}}$ (m <sup>2</sup> /g)	$S_{\text{meso}}$ (m <sup>2</sup> /g)	$S_{\text{micro}}$ (m <sup>2</sup> /g)	$V_{\text{meso}}$ (cm <sup>3</sup> /g)	$V_{\text{micro}}$ (cm <sup>3</sup> /g)	$V_{\text{tot}}$ (cm <sup>3</sup> /g)
AC	2081	246	1835	0.8129	0.9823	1.262
AC12	1916	176	1739	0.7293	0.9328	1.145
AC10	1805	191	1641	0.6760	0.8646	1.080
AC8	1760	172	1588	0.6836	0.8516	1.058
AC6	1750	184	1566	0.6722	0.8438	1.052

### Electrochemical Characteristics

The samples were investigated further as the electrodes of supercapacitors. A test of electrochemical performance was performed in a 7.0 mol/L KOH electrolyte. The galvanostatic charge–discharge, specific capacitance at different current densities, cyclic voltammeteries (CV), and alternating current impedances were studied in order to determine the effect of sulfur loading on electrodes, as shown in Figs. 6 through 9. The galvanostatic charge-discharge curves of the AC and SAC electrodes, at a current density of 50 mA/g, are presented in Fig. 6. The shape of the curves for all of the samples was triangular, which confirmed that the ideal capacitive behavior was nearly symmetric for the charge/discharge curves. The corresponding specific capacitance value, at a current density of 50 mA/g, was calculated according to the following equation,

$$C_m = \frac{I \times \Delta t}{\Delta V \times m} \quad (1)$$

where  $C_m$  is the specific capacitance per mass weight of activated carbon in the electrode (F/g),  $I$  is the discharge current (A),  $\Delta t$  is the time elapsed for the discharge branch from 0 to 1 V (s),  $\Delta v$  is the voltage difference within the time (V), and  $m$  is the active mass of carbon on the electrode (g).

The specific capacitance of the samples varied from 245 to 264 F/g (AC: 245 F/g, AC12: 259 F/g, AC10: 264 F/g, AC8: 255 F/g, and AC6: 252 F/g) under a current density of 50 mA/g. Heteroatom doping could have induced pseudo-capacitance, thus enhancing the entire capacitance of the carbon materials. The contribution of S-containing groups to pseudo-capacitance could be concluded from Tables 1 and 2. Generally, as the specific surface area of the substrate increased, the capacitance also increased. However, compared with AC and AC12, which possess larger specific surface areas, sample AC10 exhibited a greater capacitance because of the larger degree of pseudo-capacitance. Although samples AC8 and AC6 possessed higher sulfur content, the specific capacitance of these samples was lower than AC10 because of the smaller specific surface area. Compared with the AC sample, SAC samples exhibited higher specific capacitance after sulfur modification, and sample AC10 exhibited the highest specific capacitance of 264 F/g. According to the specific surface area and pore size distribution of the samples shown in Table 3, when the sulfur content reached 1.64% (Table 2), the contribution to pseudo-capacitance of sulfur is optimal and the sulfur function dominates the specific capacitance over the effect of the pore structure. Consequently, the synergistic effect of pseudo-capacitance and pore structure reached an optimum level when the carbon-sulfur ratio was 10:1, which was also the highest specific capacitance. Because of this result, sulfur-doping exhibited a positive effect on the enhancement of capacitance.

Figure 7 illustrates the specific capacitance of electrodes at various current densities ranging from 50 mA to 5 A/g within a potential window from 0 to 1 V. The sudden potential drop at the beginning of the constant current discharge (IR drop) could be attributed to the resistance of electrolyte solution and the inner resistance of ion diffusion (Shang *et al.* 2014). Cyclic voltammetry (CV) testing (Fig. 8) showed rectangular curves from 0 to 1.0 V, at a scanning rate of 1.0 mV/s to 200 mV/s, respectively. The CV curves presented nearly rectangular shapes at different scan rates, which suggests good capacitive devices. The obvious hump during the sweep at 0.8 to 1.0 V was observed for both the AC and AC10 samples; this is evidence that complex reversible redox reactions occurred and overlapped, which is usually attributed to the involvement of sulfur and nitrogen functional groups (Tsubota *et al.* 2011). It has been widely accepted that heteroatom-containing groups have a positive effect on the electrochemical performance. Compared with the AC sample, the pseudo-faradic reactions of AC10 were more obvious from the hump in the CV curves. Therefore, apart from surface area and nitrogen functional groups, sulfur functional groups contribute greatly to the enhancement of capacitance.

Electrochemical impedance spectroscopy (EIS), also known as the Nyquist plot, can provide insight into how sulfur modification affects the performance of a sample. The Nyquist plots of AC and AC10 samples are shown in Fig. 9. The straight line in the low-frequency region and the small arc in the high-frequency region depict typical behaviors of supercapacitors. The impedance plots of both samples show almost identical shapes, with one semicircular arc in the very-high-frequency region and one linear part in the low-frequency region. The intercept at the real axis represents the equivalent series resistance (ESR) value at high frequencies, and the slope at the low-frequency region reflects the diffusive resistivity of the electrolyte ions within the pores. The straight line

portion of AC10 close to the imaginary axis (y-axis) suggests that AC10 has better capacitive behavior than AC. The semicircular arc of AC10 is slightly decreased in size compared with that of AC, and the ESR values of AC10 and AC are approximately 0.16 and 0.24, respectively, revealing a decrease in the charge-transfer resistance.

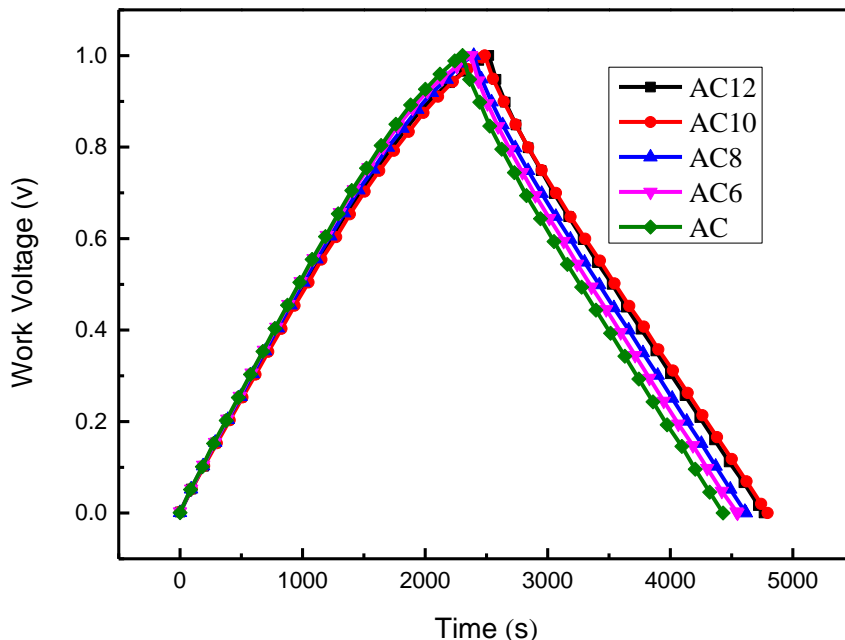


Fig. 6. Charge-discharge curves of electrodes in 7.0 M KOH at a constant current density of 50 mA/g

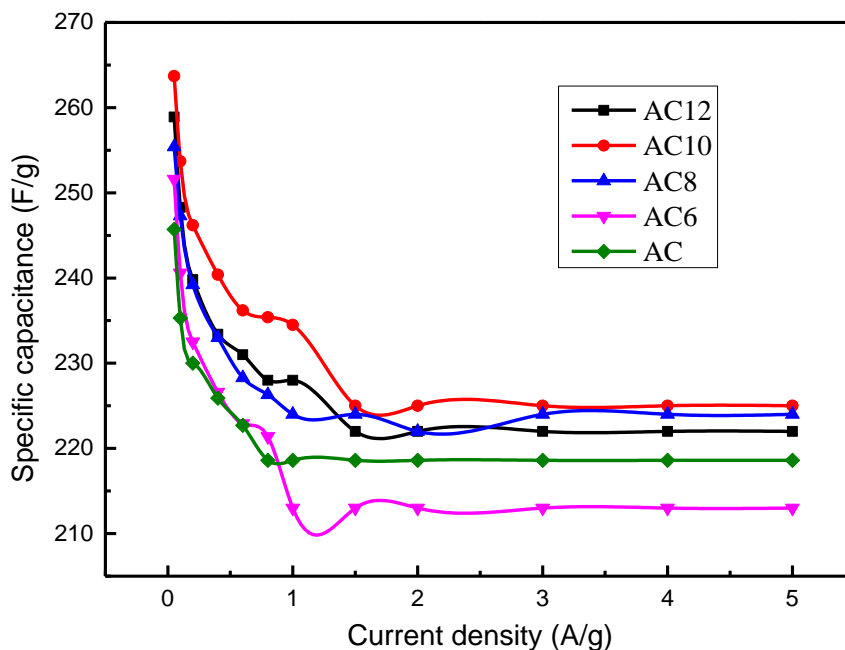
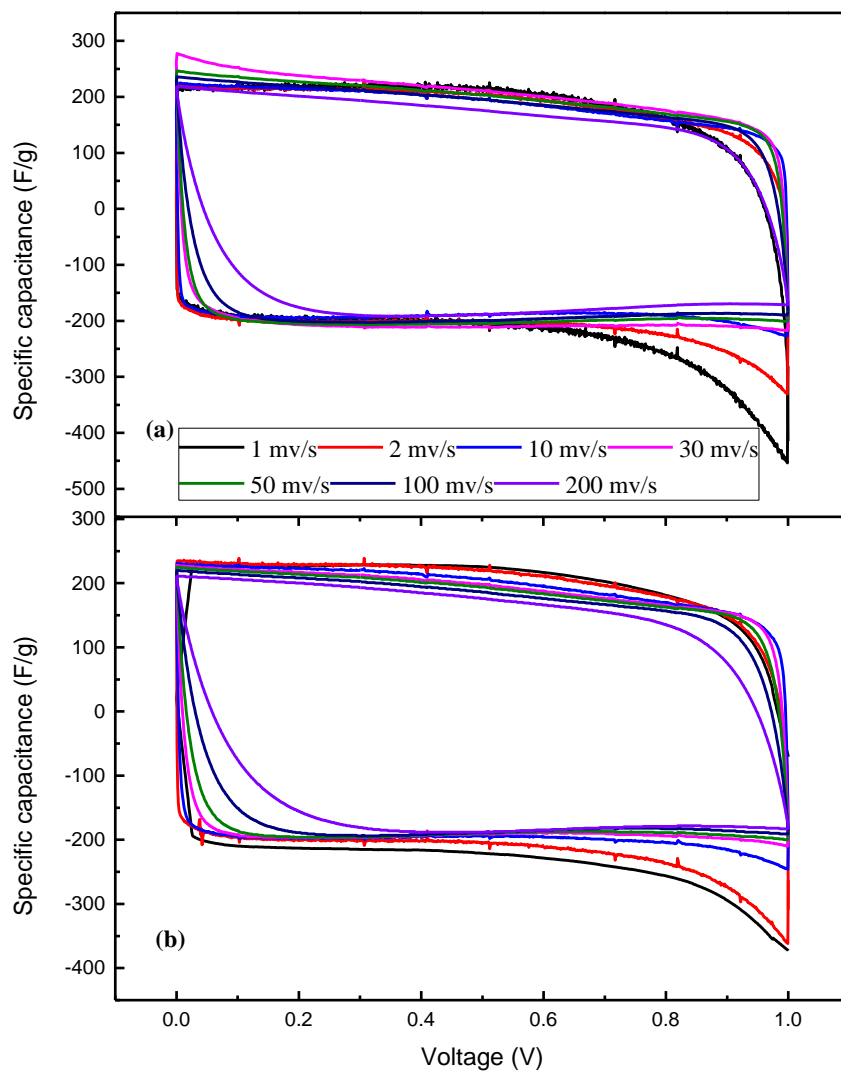
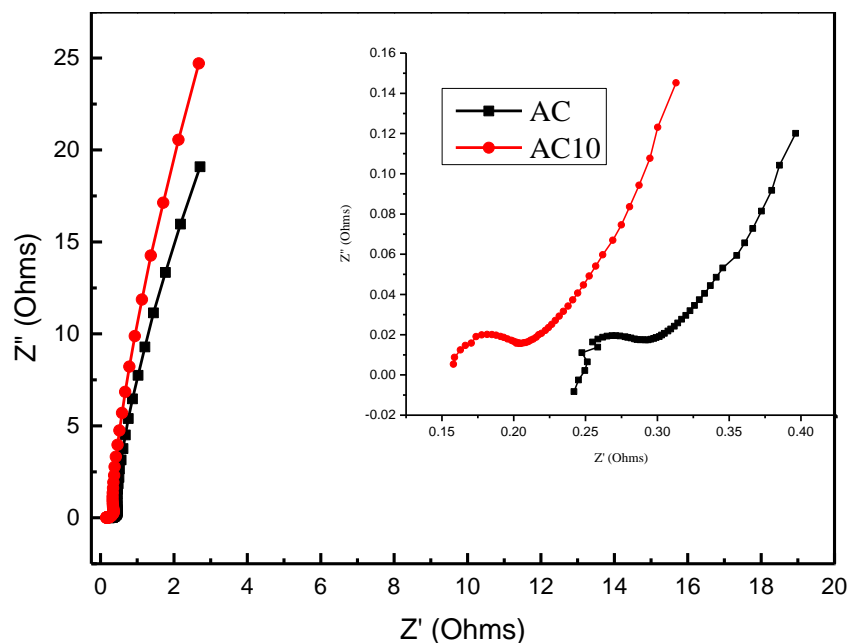


Fig. 7. Calculated specific capacitance as a function of current density of electrodes



**Fig. 8.** Cyclic voltammograms of (a) AC10 and (b) AC electrodes in 7.0 M KOH at different scanning rates



**Fig. 9.** Nyquist plot of AC and AC10 electrodes (inset: enlarged high-frequency region of the Nyquist plot)

## CONCLUSIONS

1. This work disclosed a simple and efficient method for the production of N-, S-co-doped mesoporous and microporous carbons. The specific surface area of SAC samples showed an obvious reduction compared with the AC sample; however, the modification of nitrogen-containing activated carbon with sulfur was shown to increase the capacitance of electrodes for supercapacitor applications, deduced from the electrochemical measurements.
2. The XPS test demonstrated that the enhancement in the electrochemical property for the N-, S-co-doped carbon materials was mainly attributable to the thiophene and sulfone sulfur-containing groups. The SAC electrode exhibited the highest specific capacitance of 264 F/g at a current density of 50 mA/g, when the ratio of C:S was 10:1.
3. Nitrogen-, S-co-doped activated carbon from waste MDF is a good choice as a supercapacitor because it is low-cost and eco-friendly. The present work contributed valuable information towards the development of N-, S-co-doped carbon with high specific surface areas and excellent electrochemical performance properties from bio-waste materials.

## ACKNOWLEDGMENTS

The authors are greatly indebted to the National Natural Science Funding under Project: 51572028

## REFERENCES CITED

- Djurfors, B., Broughton, J., Brett, M., and Ivey, D. (2003). "Microstructural characterization of porous manganese thin films for electrochemical supercapacitor applications," *Journal of Materials Science* 38(24), 4817-4830. DOI: 10.1023/B:JMISC.0000004401.81145.b6
- Faraji, S., and Ani, F. N. (2015). "The development supercapacitor from activated carbon by electroless plating – A review," *Renewable and Sustainable Energy Reviews* 42, 823-834. DOI: 10.1016/j.rser.2014.10.068
- Ferrero, G. A., Fuertes, A. B., and Sevilla, M. (2015). "N-doped porous carbon capsules with tunable porosity for high-performance supercapacitors," *Journal of Materials Science A* 3(6), 2914-2923. DOI: 10.1039/c4ta06022a
- Gao, F., Qu, J., Zhao, Z., Wang, Z., and Qiu, J. (2016). "Nitrogen-doped activated carbon derived from prawn shells for high-performance supercapacitors," *Electrochimica Acta* 190, 1134-1141. DOI: 10.1016/j.electacta.2016.01.005
- Gu, W., Sevilla, M., Magasinski, A., Fuertes, A. B., and Yushin, G. (2013). "Sulfur-containing activated carbons with greatly reduced content of bottle neck pores for double-layer capacitors: A case study for pseudocapacitance detection," *Energy and Environmental Science* 6(8), 2465-2476. DOI: 10.1039/c3ee41182f
- Hasegawa, G., Aoki, M., Kanamori, K., Nakanishi, K., Hanada, T., and Tadanaga, K. (2011). "Monolithic electrode for electric double-layer capacitors based on macro/meso/microporous S-containing activated carbon with high surface area," *Journal of Materials Chemistry* 21(7), 2060-2063. DOI: 10.1039/c0jm03793a
- Huang, Y., Candelaria, S. L., Li, Y., Li, Z., Tian, J., Zhang, L., and Cao, G. (2014). "Sulfurized activated carbon for high energy density supercapacitors," *Journal of Power Sources* 252, 90-97. DOI: 10.1016/j.jpowsour.2013.12.004
- Inal, I. I. G., Holmes, S. M., Banford, A., and Aktas, Z. (2015). "The performance of supercapacitor electrodes developed from chemically activated carbon produced from waste tea," *Applied Surface Science* 357(1), 696-703. DOI:10.1016/j.apsusc.2015.09.067
- Nolan, H., McEvoy, N., Keeley, G. P., Callaghan, S. D., McGuinness, C., and Duesberg, G. S. (2013). "Nitrogen-doped pyrolytic carbon films as highly electrochemically active electrodes," *Physical Chemistry Chemical Physics* 15(42), 18688-18693. DOI: 10.1039/c3cp53541j
- Sari, F. N. I., and Ting, J.-M. (2015). "One step microwaved-assisted hydrothermal synthesis of nitrogen doped graphene for high performance of supercapacitor," *Applied Surface Science* 355(15), 419-428. DOI: 10.1016/j.apsusc.2015.07.123
- Sevilla, M., and Fuertes, A. B. (2012). "Highly porous S-doped carbons," *Microporous and Mesoporous Materials* 158, 318-323. DOI: 10.1016/j.micromeso.2012.02.029
- Shang, T.-X., Zhang, M.-Y., and Jin, X.-J. (2014). "Easy procedure to prepare nitrogen-containing activated carbons for supercapacitors," *RSC Advances* 4(73), 39037-36044. DOI: 10.1039/c4ra05881j
- Shang, T. X., Cai, X. X., and Jin, X. J. (2015). "Phosphorus- and nitrogen-co-doped particleboard based activated carbon in supercapacitor application," *RSC Advances* 5(21), 16433-16438. DOI: 10.1039/c5ra00142k
- Si, W., Zhou, J., Zhang, S., Li, S., Xing, W., and Zhuo, S. (2013). "Tunable N-doped or dual N, S-doped activated hydrothermal carbons derived from human hair and

- glucose for supercapacitor applications," *Electrochimica Acta* 107, 397-405. DOI: 10.1016/j.electacta.2013.06.065
- Tsubota, T., Takenaka, K., Murakami, N., and Ohno, T. (2011). "Performance of nitrogen- and sulfur-containing carbon material derived from thiourea and formaldehyde as electrochemical capacitor," *Journal of Power Sources* 196(23), 10455-10460. DOI: 10.1016/j.jpowsour.2011.07.025
- Wang, B., Qiu, J., Feng, H., Sakai, E., and Komiyama, T. (2016). "KOH-activated nitrogen doped porous carbon nanowires with superior performance in supercapacitors," *Electrochimica Acta*, 190, 229-239. DOI: 10.1016/j.electacta.2016.01.038
- Zhao, X., Zhang, Q., Chen, C.-M., Zhang, B., Reiche, S., Wang, A., Zhang, T., Schlögl, R., and Su, D. S. (2012). "Aromatic sulfide, sulfoxide, and sulfone mediated mesoporous carbon monolith for use in supercapacitor," *Nano Energy* 1(4), 624-630. DOI: 10.1016/j.nanoen.2012.04.003
- Zhou, Y., Candelaria, S. L., Liu, Q., Huang, Y., Uchaker, E., and Cao, G. (2014). "Sulfur-rich carbon cryogels for supercapacitors with improved conductivity and wettability," *Journal of Materials Chemistry A* 2(22), 8472-8482. DOI: 10.1039/c4ta00894d

Article submitted: January 9, 2016; Peer review completed: February 19, 2016; Revisions accepted: March 9, 2016; Published: March 17, 2016.

DOI: 10.15376/biores.11.2.4055-4068